Talanta 129 (2014) 529–538

Contents lists available at ScienceDirect

Talanta

journal homepage: www.elsevier.com/locate/talanta

# High-performance liquid chromatographic and mass spectrometric analysis of fluorescent carbon nanodots

Xiaojuan Gong [a,1], Qin Hu [b], Man Chin Paau [b], Yan Zhang [a,2], Lei Zhang [a,1], Shaomin Shuang [a], Chuan Dong [a,*], Martin M.F. Choi [b,**]

[a] Institute of Environmental Science, and School of Chemistry and Chemical Engineering, Shanxi University, Taiyuan 030006, China
[b] Partner State Key Laboratory of Environmental and Biological Analysis, and Department of Chemistry, Hong Kong Baptist University, 224 Waterloo Road, Kowloon Tong, Hong Kong, China

ARTICLE INFO

*Article history:*
Received 21 January 2014
Received in revised form
4 April 2014
Accepted 5 April 2014
Available online 18 April 2014

*Keywords:*
Analytical separation
Carbon dots species
Chitosan

ABSTRACT

Amino/hydroxyl-functionalized fluorescent carbon nanodots (C-NanoD) are conveniently synthesized based on hydrothermal carbonization of chitosan at 180 °C. Dialysis membranes with small cut-off masses (500–1000 Da) were found useful for removing the side-products and low molecular mass species to purify the C-NanoD product. Herein, reversed-phase high-performance liquid chromatography (RP-HPLC) has been successfully applied to fractionate the C-NanoD product. The elution order of the C-NanoD species present in the sample follows approximately their core sizes from small to large. The separated C-NanoD fractions are collected and characterized by UV absorption spectroscopy, photoluminescence (PL) spectroscopy, matrix-assisted laser desorption/ionization time-of-flight mass spectrometry (MALDI-TOF MS), and transmission electron microscopy (TEM). All the C-NanoD fractions display a distinctive absorption band at 300 nm, attributing to the $n \rightarrow \pi^*$ transition of C=O bond. The PL spectra of the fractions display emission peaks at 400–415 nm which are slightly red-shifted with their increase in relative molecular masses. The C-NanoD fractions are fully anatomized by MALDI-TOF MS, displaying their fragmentation mass ion features. The core sizes of some selected C-NanoD are determined as 1.6, 1.8, 2.5, and 3.1 nm by TEM which are in consistent with their HPLC elution order. The findings highlight the virtues of RP-HPLC to fractionate and reveal the unique characteristics of individual C-NanoD species present in an as-synthesized C-NanoD product which may have potential applications in the fields of bioanalysis, bioimaging, catalysis, chemosensing, energy storage, and optoelectronics device.



## 1. Introduction

In recent years there is a huge interest in carbon nanodots (C-NanoD) primarily because of their unique properties in chemical inertness, good stability without photo-bleaching and optically non-blinking [1,2] size- and wavelength-dependent luminescence emission [2], ease of synthesis and excellent biocompatibility [3,4], low toxicity [5], cost-effective raw materials [6], promising up-conversion property [7,8], and environmental friendliness [9] in comparison to conventional semiconductor quantum dots (QDs). Small C-NanoD are one of the latest rising stars among the carbon nanomaterial family, which upon surface functionalization by organic molecules were found to exhibit bright and colorful fluorescence emissions [10]. Most notably, they have the potential to replace the currently used toxic semiconductor-based QDs. However, this fluorescent C-NanoD is not well studied as compared to other carbon nanomaterials such as carbon nanotubes, fullerenes and graphenes. The understanding of the origin of fluorescence in C-NanoD is still under investigation. Sun et al. [10] and Wang et al. [11] proposed that the fluorescence emission in C-NanoD is attributed to radiative recombination of the photo-induced electron and hole that is confined to the carbon nanoparticle (NP) surface. This resembling phenomenon is found in nanoscale semiconductors [12]. Baker and Colón [13] suggested that the surface groups have strong influence on the fluorescence emission of C-NanoD which is derived from the surface energy trap state. Their size-dependent photophysical properties still require considerable attention.

So far considerable effort has been dedicated to the synthesis of various functionalized and non-functionalized C-NanoD based on thermal oxidation of suitable molecular precursors [14,15], combustion of carbon soot [16] or natural gas [17], laser ablation or

* Corresponding author. Tel./fax: +86 351 7018613.
** Corresponding author. Tel.: +852 34117839; fax: +852 34117348.
*E-mail addresses:* dc@sxu.edu.cn (C. Dong), mfchoi@hkbu.edu.hk (M.M.F. Choi).
[1] Exchange students.
[2] Postdoctoral research fellow on visit to Hong Kong Baptist University.

http://dx.doi.org/10.1016/j.talanta.2014.04.008
0039-9140/

electrochemical oxidation of graphite [18,19], microwave-heating of sucrose [20,21], and thermal degradation of polysaccharides [22,23]. The fundamental studies and applications of C-NanoD have also aroused intensive interest. Although great effort has been made in improving the quantum yield ($\Phi_S$) and surface functionalization of C-NanoD, not much focus is spent on the analytical separation of fluorescent C-NanoD. We suspect that most C-NanoD samples synthesized to date are in fact mixtures containing various core sizes, shapes and surface-functionalized moieties of C-NanoD species; in other words, an as-synthesized C-NanoD product only represents the summation or average properties of its individual C-NanoD species. In theory, each unique C-NanoD species should bear its own distinct chemical and physical properties which require more precise and accurate studies. To our knowledge, there are only few reports on the separation of C-NanoD. Liu et al. [16] fractionated C-NanoD by gel electrophoresis. C-NanoD samples derived from soot were analyzed by capillary electrophoresis (CE) [13] and anion-exchange ion chromatography (AEIC) [24,25]. Gel electrophoresis does not provide high separation efficiency. Although CE can enjoy excellent separation, the separated and collected fractions are minuscule which make further characterization difficult. The AEIC approach has an immediate impact on the analysis and fractionation of various other nanomaterials; however, it requires relatively expensive ion-exchange column and ammonium acetate or carbonate as the eluent. The separation largely depends on the pH of eluent and the search of the optimal separating condition is time-consuming. In addition, AEIC only separates charged components but not the neutral C-NanoD entities. The buffers for eluting the samples have to be removed from the collected fractions prior to mass spectral analysis and other characterizations. As such, there is a need to develop other better analytical separation techniques to fractionate C-NanoD.

Herein, we firstly report a reversed-phase high-performance liquid chromatographic (RP-HPLC) method for efficient separation and isolation of amino/hydroxyl-functionalized fluorescent C-NanoD fractions from an as-synthesized C-NanoD product. More importantly, RP-HPLC allows for the collection of C-NanoD fractions with scale-up capabilities. It is relatively easy to remove the solvents from the collected HPLC fractions for further characterizations. Baker and Baker [2] proposed that there is a demand for developing better synthetic routes and more detailed fundamental studies of C-NanoD properties. By collecting the separated fractions, the UV–vis absorption, photoluminescence (PL), matrix-assisted laser desorption/ionization time-of-flight mass spectra (MALDI-TOF MS) and transmission electron microscopic (TEM) images of each C-NanoD fraction can be realized. It is well known that C-NanoD possesses the size-dependent photophysical properties [26]. An understanding of the chromatographic separation of C-NanoD will not only help establish composition-synthesis correlations of as-synthesized C-NanoD but will also provide useful information for photophysical and chemical properties of each C-NanoD fraction. This information can provide important insights in catalysis and nanoscale electronic device research. Our developed RP-HPLC technology could open up new initiatives on extensive studies of individual C-NanoD species in the biomedical, catalysis, electronic and optical device, energy storage, material, and sensing fields. It can also provide a methodology to select and harvest the most fluorescent C-NanoD fractions for bioimaging, biosensing and optoelectronics device applications.

## 2. Experimental

### 2.1. Chemicals and reagents

Chitosan (85%, 100–300 kDa) was acquired from Chengdu Kelong Chemical Reagent Factory (Chengdu, China). Glacial acetic acid was obtained from Chengdu Chemical Plant (Chengdu, China). HPLC-grade methanol (MeOH) was purchased from Labscan (Bangkok, Thailand). 2,5-Dihydroxybenzoic acid (DHB, 98%) was from Sigma (St. Louis, MO, USA). Water was purified through a Milli-Q-RO4 water purification system (Millipore, Bedford, MA, USA) with a resistivity higher than 18 MΩ cm. All reagents of analytical reagent grade or above were used as received.

### 2.2. C-NanoD sample preparation

Amino/hydroxyl-functionalized fluorescent C-NanoD samples were synthesized according to a literature method with slight modifications [23]. In brief, chitosan was mixed with glacial acetic acid in a Teflon equipped stainless steel acid digestion vessel which was then sealed and placed in a muffle furnace for hydrothermal treatment at 180 °C for 12 h. After the reaction, the vessel was cooled down to obtain the dark brown solid. The synthetic details are deposited in Supplementary data. The crude product was then dissolved in water and sonicated in a water bath for 1 h. The obtained dark brown solution was centrifuged at 13,000 rpm for 15 min to remove the deposits. The supernatant was collected and further purified by dialysis with a Spectrum Laboratories cellulose ester dialysis membrane tube (molecular weight cut off 500–1000 Da) (Rancho Dominguez, CA, USA) in 2 L of Milli-Q water for three days. The C-NanoD solution was collected from the dialysis membrane tube and freeze-dried to obtain the C-NanoD product.

### 2.3. Instrumentation

The UV–vis absorption spectrum of the as-prepared C-NanoD product was acquired with a Varian Cary 300 scan UV–vis absorption spectrophotometer (Palo Alto, CA, USA) at 225–500 nm. The PL spectra of the as-prepared C-NanoD and the collected HPLC C-NanoD fractions were determined on a Photon Technology International QM4 spectrofluorometer equipped with a photomultiplier tube detector (Birmingham, NJ, USA). $\Phi_S$ of the as-prepared C-NanoD was determined by comparing the integrated PL intensities and absorbances of C-NanoD with quinine sulfate as the reference (Fig. S1 in Supplementary data). The experimental details of $\Phi_S$ determination of the as-prepared C-NanoD and C-NanoD fractions are deposited in Supplementary data.

The Fourier transform infrared (FTIR) spectra of the as-prepared solid amino/hydroxyl-functionalized fluorescent C-NanoD product and raw reagent chitosan were obtained from a Nicolet Magna 550 FTIR spectrometer (Thermo Scientific, West Palm Beach, FL, USA) with the potassium bromide (KBr) pellet technique ranging 500–3700 $cm^{-1}$. The C-NanoD/KBr and chitosan/KBr disks were obtained by mixing few milligrams of C-NanoD and chitosan with ~100 mg KBr powder, respectively, grinding to approximately 2 μm in an agate mortar, and subjecting to 29.7 MPa pressure by a pressing machine.

### 2.4. HPLC separation

Chromatographic separation was conducted on a Waters (Milford, MA, USA) instrument comprising a 2695 separations module capable of gradient elution, a 2996 photodiode array detector and a 2475 multi-wavelength fluorescence detector. Absorption chromatogram was taken at 300 nm while fluorescence chromatogram was obtained at excitation/emission wavelengths of 300/405 nm. Absorption spectra (1.2 nm resolution) of the separated C-NanoD peaks were in situ captured at 225–390 nm. An Agilent TC-C18 chromatographic column (4.6 mm i.d. × 250 mm) packed with 5 μm octadecyl-bonded silica (C18) with 130 Å pore size (Santa

Clara, CA, USA) was used for separation of C-NanoD. The aqueous C-NanoD sample solutions (1.0 mg/mL) were pre-filtered through the Alltech 0.2 μm cellulose acetate membrane syringe filters (Deerfield, IL, USA) before injections.

The mobile phase containing MeOH and Milli-Q water was filtered through 0.45 μm cellulose acetate membrane filters (Alltech) prior to use. The injection volume was 20 μL and the column temperature was maintained at 25 °C. A gradient elution program was applied at a flow rate of 0.80 mL/min as follows: 0.0% v/v MeOH linearly increased to 3.0% v/v MeOH from 0.0 to 30 min and then 3.0% v/v MeOH linearly increased to 5.0% v/v MeOH from 30 to 60 min. The selected HPLC fractions were collected manually based on the appropriate UV signal threshold. The collected HPLC C-NanoD fractions were purged and pre-concentrated by a stream of $N_2$ at room prior to PL, MS and TEM studies.

### 2.5. Characterization of HPLC fractions

The concentrated HPLC C-NanoD fractions were analyzed by a Bruker Autoflex MALDI-TOF mass spectrometer (Bremen, Germany). Each fraction was mixed with a 1.0 M solution of DHB in MeOH/water (1:1 v/v), respectively. Then 4.0 μL of this mixture was deposited on a MALDI target plate and air-dried. The sample was irradiated by a pulsed $N_2$ laser working at 337 nm (3 ns pulse, 3 Hz). In general, 30 laser shots were averaged for each spectrum.

The TEM images of selected concentrated HPLC fractions were obtained with a JEOL JEM-1011 transmission electron microscope (Tokyo, Japan) operating at 200 kV. Samples were prepared by casting and evaporating a droplet of aqueous solution of HPLC fraction onto Agar Scientific 400 mesh copper grids (Stansted, Essex, UK). Particle size was determined by the ImageJ 1.47 software (National Institutes of Health, Bethesda, MD, USA).

## 3. Results and discussion

### 3.1. Characterization of C-NanoD product

C-NanoD has been employed for bioimaging in various live cells because of their bright and stable fluorescence, good water-solubility, biocompatibility, and nontoxicity [3–5]. Water-soluble amino/hydroxyl-functionalized fluorescent C-NanoD sample was synthesized by carbonizing a mixture of chitosan and glacial acetic acid at a mild temperature of 180 °C with $\Phi_S$ of 7.20%. Fig. 1A displays the UV–vis absorption spectra of the reagents chitosan/acetic acid ((a) red line) and the as-prepared C-NanoD ((b) black line). The absorption of chitosan/acetic acid starts only below 250 nm whereas the C-NanoD displays strong UV absorption with a small shoulder peak at 260 nm and a major peak at 300 nm, corresponding to the $\pi \rightarrow \pi^*$ transition of aromatic C=C bond and $n \rightarrow \pi^*$ transition of C=O bond, respectively [27–29]. In addition, C-NanoD shows a strong emission peak at 414 nm (Fig. 1(c), blue line) upon excitation at 340 nm, whereas the reagents chitosan and acetic acid do not show any fluorescence in the UV–vis region. The UV–vis and PL spectral signature demonstrates that chitosan/acetic acid has been carbonized into C-NanoD by a mild hydrothermal route. The inset in Fig. 1 depicts the photographic images of the chitosan/acetic acid and C-NanoD solutions under daylight and UV irradiation. C-NanoD solution is clear transparent yellowish brown, exhibiting strong blue luminescence under illumination of UV (365 nm) whereas chitosan/acetic acid is colorless.

The excitation-dependent PL behavior of our as-prepared C-NanoD was observed. The PL peak gradually red-shifts from 408 to 419 nm when the excitation wavelength moves from 300 to 330 nm as depicted in Fig. 1B. This observation is in consistent with most fluorescence carbon nanomaterials. This excitation wavelength-dependent PL property is commonly explained by the variation of C-NanoD product in composition, structure, particle size, and "giant red-edge effect" [14,16,23,30–34]. As far

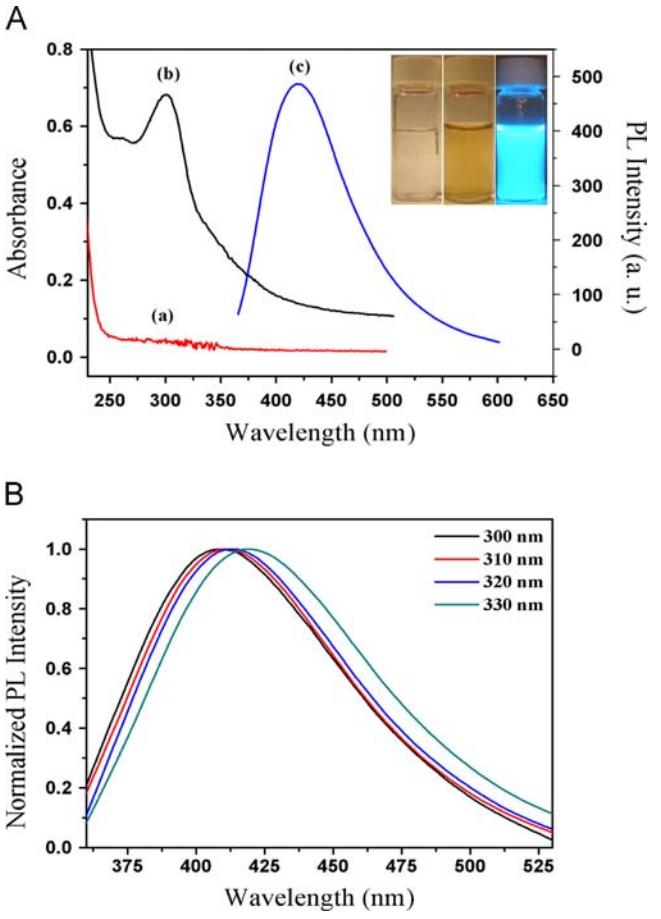


**Fig. 1.** (A) UV–vis absorption spectra of aqueous solutions of (a) chitosan and acetic acid and (b) as-synthesized C-NanoD product (c) PL spectrum of the as-synthesized C-NanoD at an excitation wavelength of 340 nm. The inset displays the photographic images of solutions of chitosan and acetic acid under daylight (left), and the as-synthesized C-NanoD under daylight (middle) and a UV (365 nm) lamp irradiation (right). (B) The normalized PL spectra of C-NanoD at different excitation wavelengths (300–330 nm).

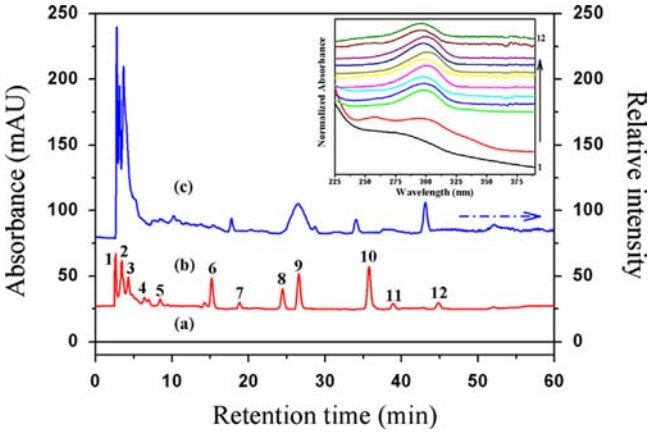


**Fig. 2.** Absorption chromatograms of (a) chitosan and acetic acid in MeOH/water (1:19 v/v) and (b) as-synthesized C-NanoD product in water monitored at 300 nm. (c) Fluorescence chromatogram of as-synthesized C-NanoD product in water monitored at excitation/emission wavelengths of 300/405 nm. Chromatograms are offset for clarity. The inset displays the absorption spectra (bottom to top) of Peaks 1–12 labeled in the absorption chromatogram. Absorbances have been normalized at 300 nm and spectra are offset for clarity.

as the PL mechanism of C-NanoD is concerned, it is believed that both surface defects, quantum size and solvent effects contribute to PL. Yang et al. considered that the formation of C-NanoD and its surface functional groups take place simultaneously during the hydrothermal carbonization process [23]. The abundant functional groups such as carboxylic acids, amines can introduce different defects on the surface which act as the excitation energy traps; thus leading to different PL properties. In principle, each C-NanoD species should possess its own spectral characteristics, depending on its core size and surface functionality.

Infrared spectroscopy is a helpful technique to characterize the surface functionality of C-NanoD. The IR spectra of pure chitosan and the as-prepared C-NanoD are depicted in Fig. S2 (Supplementary data). Chitosan exhibits the characteristic absorption bands at 3443, 2928 and 2860, 1647 and 1593, and 1120–1030 $cm^{-1}$, corresponding to the O–H and N–H stretching vibrations, C–H stretching vibrations, C–OH stretching vibrations and C–H and C–O–C bending vibrations of the pyranose ring, respectively. The as-prepared C-NanoD product shows an increase in absorption of C-N at 1400 $cm^{-1}$, representing that the amidation reaction has taken place through the dehydration process [8,23]. The O–H and N–H bonds bending vibrations of the pyranose ring at 3443 $cm^{-1}$ decrease while the CH═CH and C═O bonds corresponding to the stretching vibrations at 3100

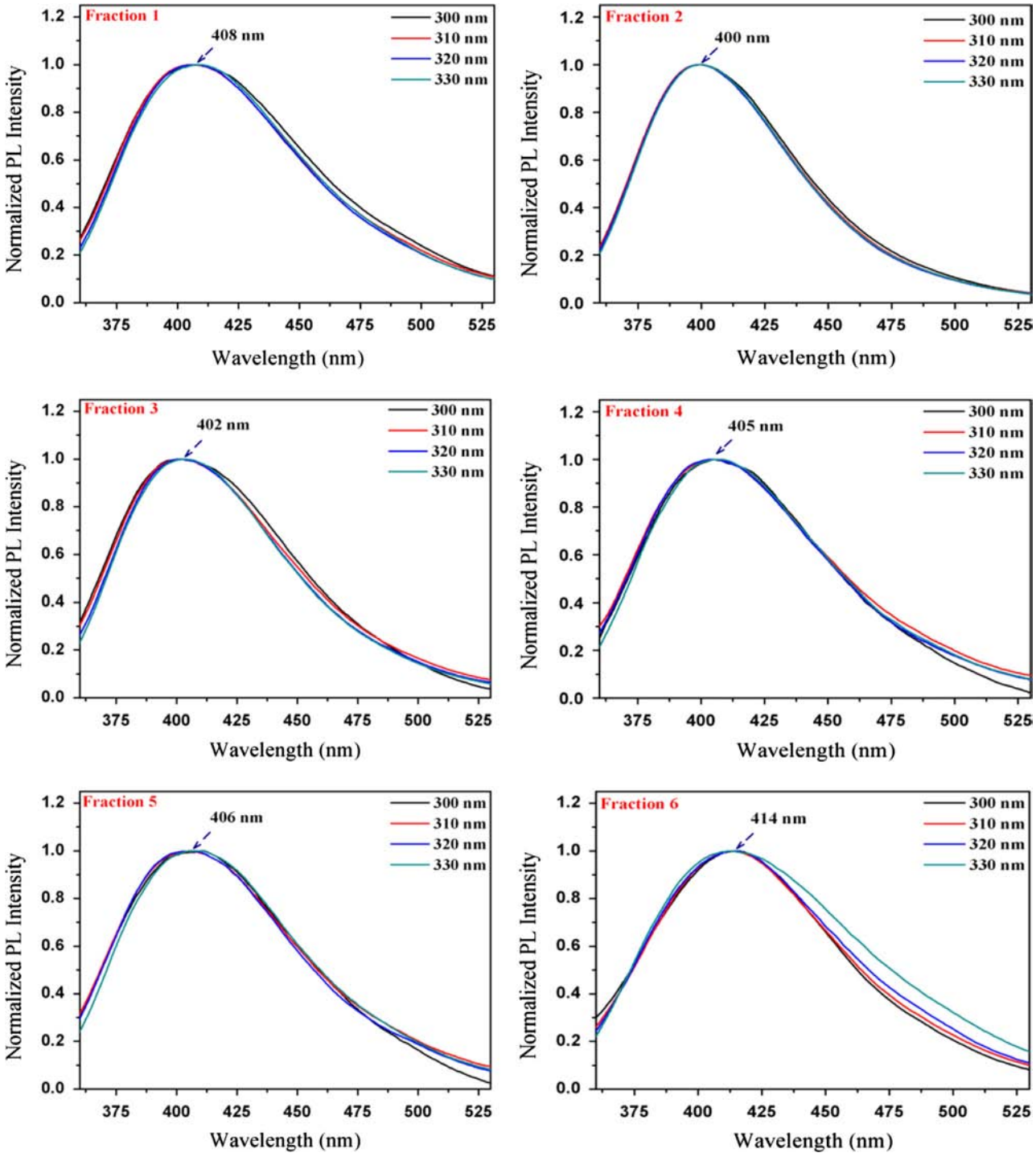


**Fig. 3.** Normalized PL spectra of Fractions 1–12 at different excitation wavelengths (300–330 nm).

and 1625 $cm^{-1}$ increase, representing chitosan and glacial acetic acid lose oxygen and hydrogen in the dehydration process. At 1030–1120 $cm^{-1}$, the C–H and C–O–C bond vibrations associated with the pyranose almost completely disappear. Again, these features can be interpreted as the degradation of the chitosan chain and the decomposition of the pyranose ring through dehydration [23]. The IR spectra suggest that the possible amidation and dehydration reactions should have taken place between chitosan and acetic acid. The resulting C-NanoD is covered with amino/hydroxyl functionalities and even some hydrolyzed chitosan single-molecule chains [8,23]. The presence of these functional groups imparts excellent water solubility of the as-synthesized C-NanoD. In essence, the hydrothermal carbonization of chitosan and glacial acetic acid mixture is an effective way of producing amino/hydroxyl-functionalized fluorescent C-NanoD which possibly comprises an olefin carbon core, surface-attached amino/hydroxyl groups and small chitosan single-molecule chains.

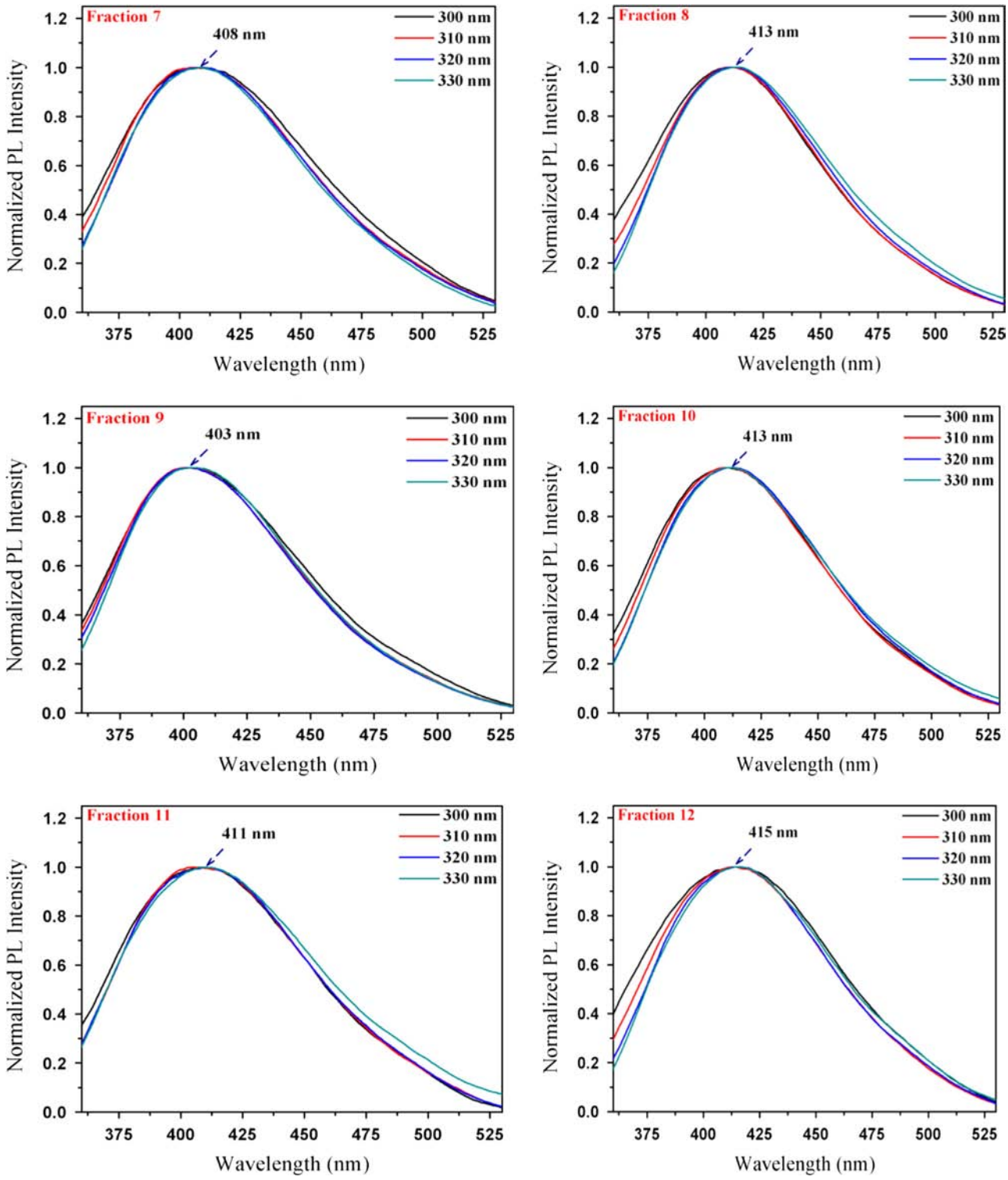


**Fig. 3.** (*continued*)

### 3.2. HPLC separation of C-NanoD sample

It has been reported that HPLC is an effective approach in separating nanomaterial mixture [35,36]. The RP-HPLC separation of C-NanoD relies on the interaction between the non-polar stationary phase and the C-NanoD. In our preliminary purification of C-NanoD product, the yellowish brown sample solution was dialyzed in membrane tubes with cut-off mass of 8000–10,000 Da. After dialysis, the solution was concentrated and analyzed by RP-HPLC. To our surprise, no chromatographic peak was found, indicating that the C-NanoD species present in the as-synthesized product must be smaller than 8000–10,000 Da and were lost during dialysis as the pore size of the membrane is too large. As such, dialysis membranes with smaller cut-off masses (500–1000 Da) were used in order to keep the C-NanoD species in the dialysis membrane tubes. Finally, numerous chromatographic peaks were evolved in the chromatograms (vide infra), inferring that the C-NanoD product indeed comprises many C-NanoD species with relative molecular masses in the range between 500–1000 and 8000–10,000 Da. In essence, dialysis membranes with smaller cut-off masses were found useful for extraction of the target C-NanoD.

It is well known that the MeOH content in mobile phase affects the chromatographic separation in a RP-HPLC system. As such, the effect of MeOH on the chromatographic behavior of the as-synthesized C-NanoD product was investigated in detail. Fig. S3

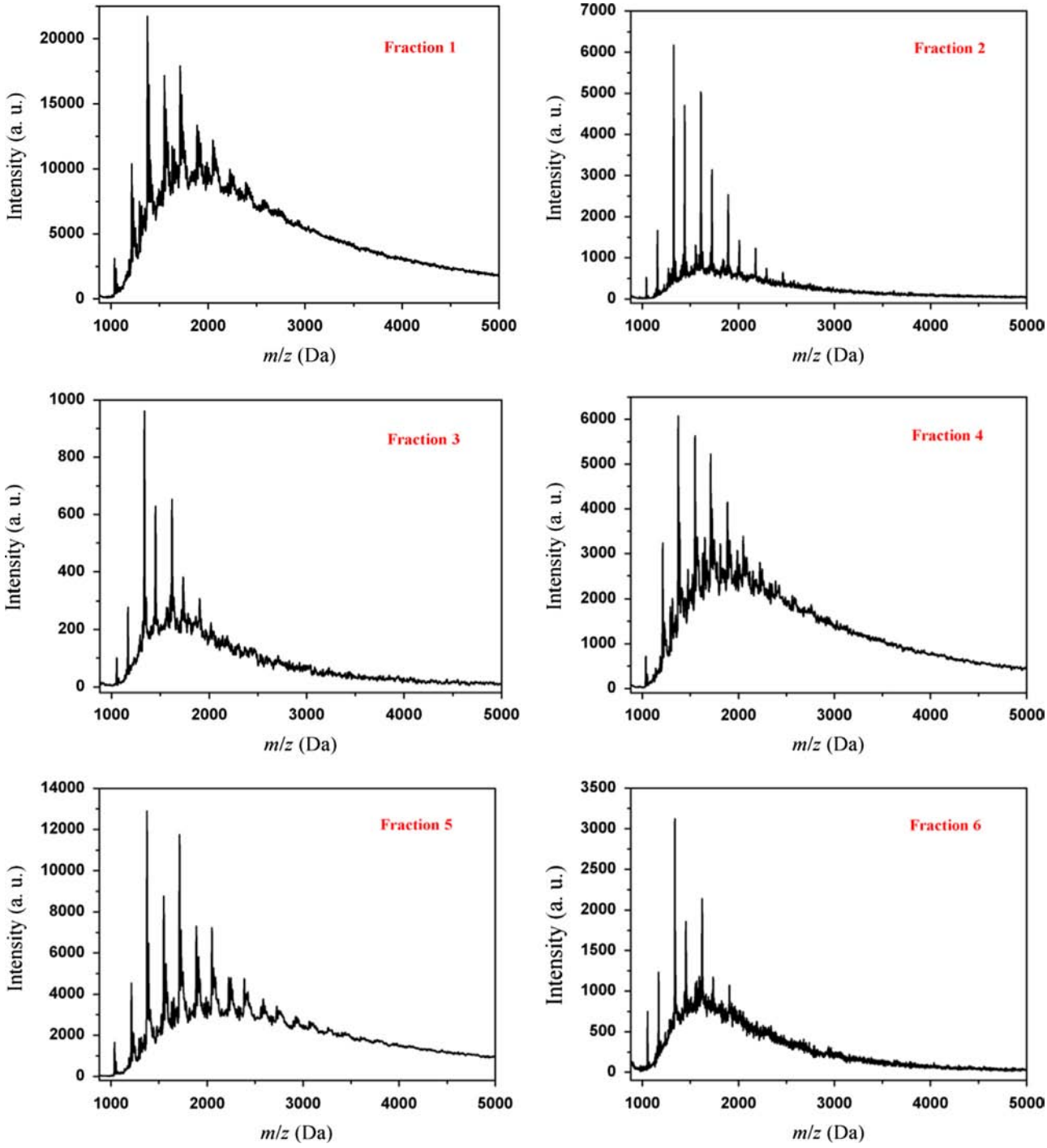


**Fig. 4.** MALDI-TOF mass spectra of Fractions 1–12.

depicts the chromatograms of the C-NanoD product obtained at various MeOH contents in the mobile phases (MeOH/water mixtures). The separation of C-NanoD is not satisfactory under the highest MeOH content (20% v/v). The chromatogram contains an earlier eluted peak and a later large broad eluted peak comprising numerous co-eluted solutes. Fortunately, these overlapping peaks could be better resolved on decreasing the concentration of MeOH to 5.0% v/v, indicating that various C-NanoD species co-exist in the as-prepared C-NanoD sample. In addition, all these resolved peaks are better retained with the decrease in MeOH content, inferring that the HPLC separation of C-NanoD follows the typical RP separation behavior of organic compounds. In summary, lowering the MeOH content in the mobile phase could improve the retention and separation of the as-prepared C-NanoD sample as this allows better hydrophobic interaction between the C-NanoD solutes and the non-polar C18 stationary phase. Thus, we conclude that the RP separation is indeed a useful approach for C-NanoD separation. However, an isocratic elution of C-NanoD sample is unsatisfactory since the C-NanoD species are either co-eluted or strongly retained on the column. As such, a solvent program was developed, starting with a lower MeOH content in the mobile phase and progressively increases to higher MeOH content to achieve good separation and totally elute all the C-NanoD solutes.

A gradient elution was developed using MeOH and water as the eluents after some preliminary experiments. Fig. 2 displays the typical absorption (curve *b*) and fluorescence (curve *c*)

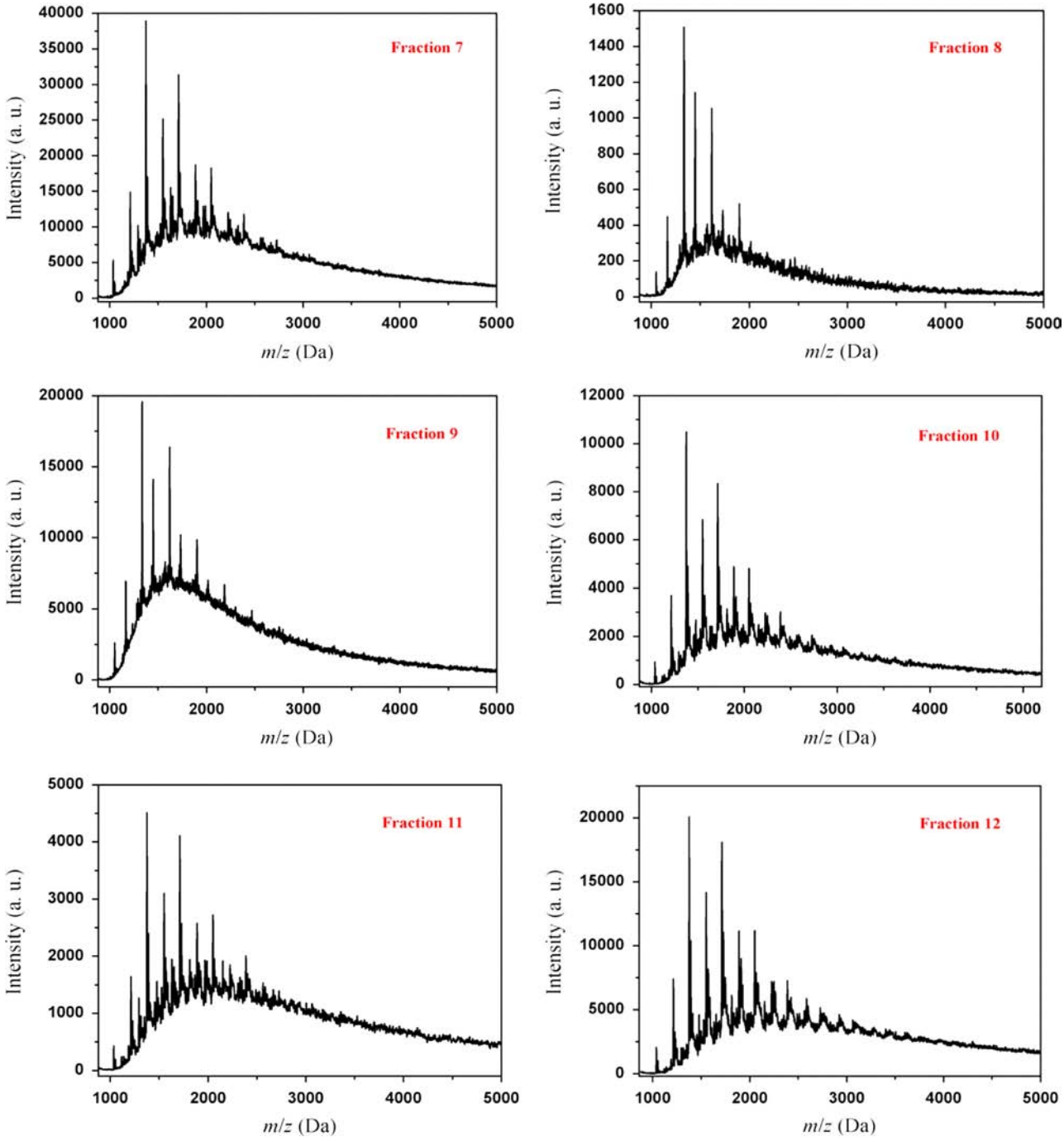


**Fig. 4.** (*continued*)

chromatograms of the as-synthesized C-NanoD product. For comparison, a chromatogram of a sample mixture of chitosan and glacial acetic acid in 1:19 MeOH/water is displayed as curve *a* in Fig. 2 and no peak is observed. It is noted that a single peak at 3.0 min is observed only when the detection wavelength is decreased to 240 nm (Fig. S4), indicating that the reagents chitosan and acetic acid do not retain on the C18 column. By contrast, numerous separated peaks are found in the absorption and fluorescence chromatograms of the C-NanoD sample (curves *b* and *c*). No peaks are eluted after 60 min for the C-NanoD sample. The combination of absorption and fluorescence detection provides corroborating as well as additional information. For examples, Peak 6 at ~15 min has a very intense UV signal but its PL signal is relatively small. Peak 12 at ~45 min has a very intense PL signal while its UV signal is small. These results indicate that the C-NanoD species possess various $\Phi_S$ ranging from 1.78% to 8.66% (Table S1 in Supplementary data) even though they are synthesized from the same reagents and synthetic conditions. Furthermore, the three major peaks at 2–5 min display both very intense UV and PL signals, representing that they are the dominant C-NanoD species in the product. Under the optimal solvent program, more later-eluted peaks are observed as compared to the chromatogram obtained from isocratic elution (Fig. S3). Totally at least 12 elution peaks are found in the chromatograms (Fig. 2). All these peaks are labeled as 1–12 and these fractions are collected for PL, MALDI-TOF MS and TEM analyses (vide infra). The quantities of the other fractions are too small to be characterized by MS and TEM and so are not studied.

The inset of Fig. 2 displays the UV–vis absorption spectra of the HPLC Fractions 1–12 (from bottom to top), revealing the spectral characteristics of these C-NanoD fractions. Most fractions show strong absorption at 300 nm. No obvious absorption bands at 250 nm are observed. The spectral feature of Fraction 2 is more distinct, having two obvious absorption bands at 257 nm and 300 nm. The bands at 257 nm concur with the small shoulder band (260 nm) in the absorption spectrum of the as-synthesized C-NanoD product (Fig. 1A(b)), originating from the $\pi \rightarrow \pi^*$ transition of the aromatic carbons on the carbon core. The 300 nm absorption band arises from the $n \rightarrow \pi^*$ transition of the surface-attached amino and hydroxyl functionalities [10,11,27–29]. The PL properties of the C-NanoD fractions are depicted in Fig. 3 and they show PL in the visible region. The emission peaks for Fractions 1–12 are between 400 and 415 nm with slight variations, attributing to their different chemical compositions, particle sizes and surface states. Interestingly, the emission peaks of the fractions do not depend much on excitation wavelength which is in contrast to the as-synthesized C-NanoD product. These results conclude that the luminescence emission property of the as-prepared C-NanoD product is excitation wavelength-dependent while its separated fractions are not under our experimental conditions. In summary, HPLC is an important and powerful tool to separate complex mixtures of C-NanoD and the spectral characteristics of the separated C-NanoD species can be truly and accurately registered.

### 3.3. Mass spectrometric analysis of C-NanoD fractions

Mass spectrometry has been an indispensable tool in chemistry and biology to determine the mass of C-NanoD and so was used to characterize Fractions 1–12 from the HPLC separation. Fig. 4 displays the *m*/*z* of Fractions 1–12. All the *m*/*z* peaks are below 4500 Da and all the peak assignments are within the *m*/*z* accuracy ($\pm$1–2 *m*/*z* units) of the MALDI-TOF MS. The highest mass ions in the MS approximately indicate the relative molecular mass of the C-NanoD species, ranging from 2700 to 4300 Da for Fractions 1–12. The RP-HPLC elution order basically follows the molecular mass of the separated C-NanoD species with some exceptions. It is well known that C-NanoD are composed of $sp^2$-hybridized carbons cores [9,17]. The increase in core size also indicates the increase in the number of carbons of the C-NanoD. In addition, it has been reported that particle size is proportional to the cube root of the mass of NP [37]. As such, stronger interaction between C-NanoD and C18 stationary phase takes place when the molecular mass (or size) of C-NanoD increases under the RP-HPLC condition. We postulate that the separation is not only governed by molecular mass or size (vide infra) but also the shape and surface-functionality of the C-NanoD.

Furthermore, each fraction displays regular mass spacings derived from the chitosan unit or its dehydration products. It is possible that the C-NanoD species were mainly comprised of carbon cores and some surface-attached chitosan moieties. The fragmented ions in MS are derived from these surface-attached chitosan moieties and carbon cores. Fig. 5A and B depicts the expanded MS of Fractions 1 and 2 at *m*/*z* range 1300–1800 and 1250–1700 Da, respectively. The inset displays the chemical formula of the mass loss of the fragmented ions. The expanded MS of Fraction 1 (Fig. 5A) shows the major *m*/*z* spacing in the alternating mass units of 175 and 163. The 175 mass spacing corresponds to the $-NH_2$ in one opening pyranose ring chitosan which reacts with a $CH_3COOH$ molecule with the loss of $-CH_2OH$ and liberates as N-(3,4-dihydroxy-1-oxopentan-2-yl)acetamide. The 163 mass spacing corresponds to one opening pyranose ring chitosan released

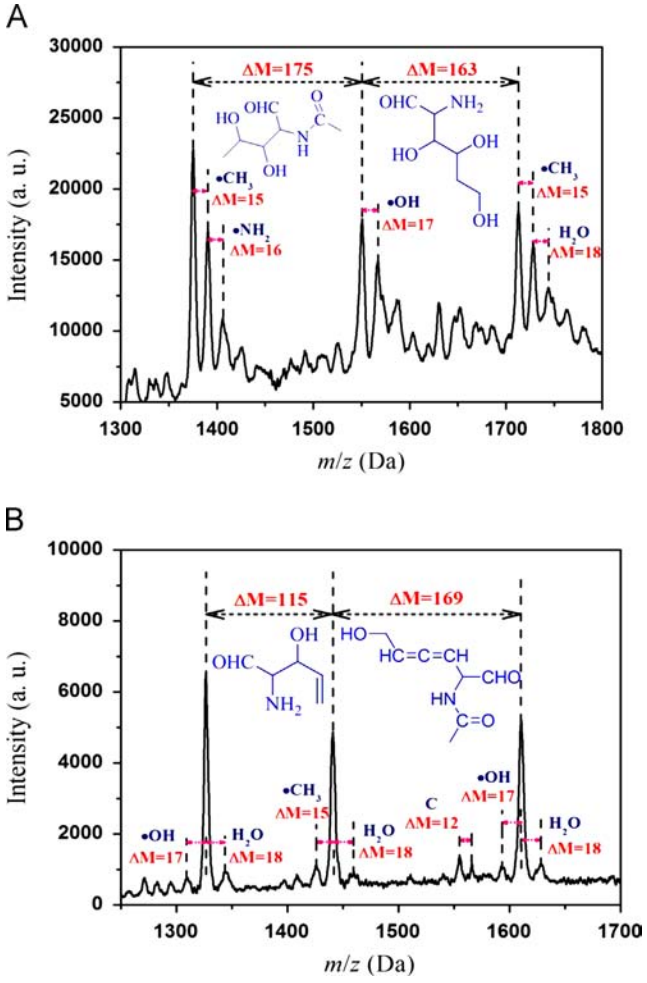


**Fig. 5.** (A) Expanded mass spectrum of Fraction 1 at *m*/*z* range 1300–1800 Da. The inset displays the chemical formula of the mass loss of 175 and 163 fragment ions. (B) Expanded mass spectrum of Fraction 2 at *m*/*z* range 1250–1700 Da. The inset displays the chemical formula of the mass loss of 115 and 169 fragment ions.

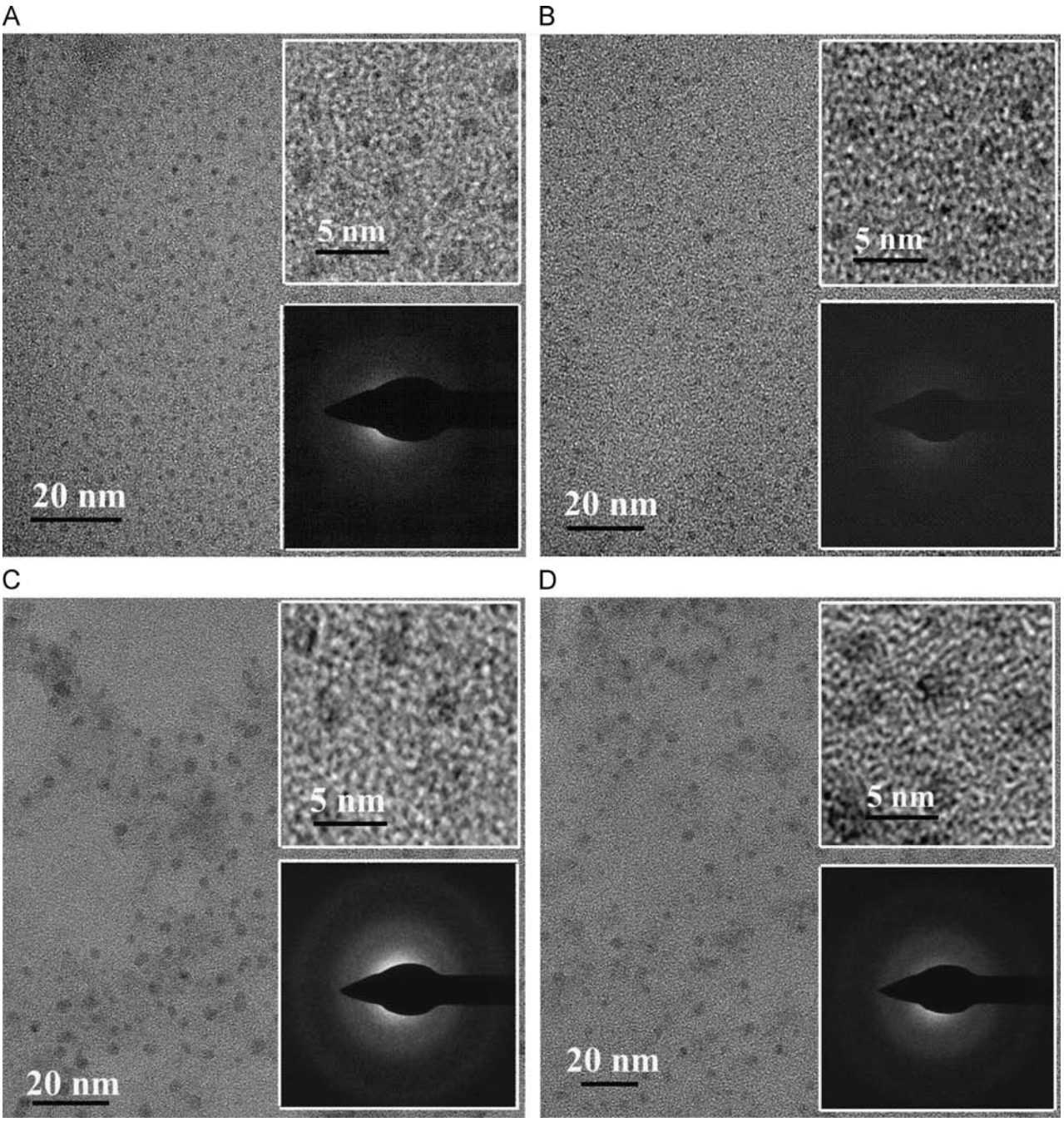


**Fig. 6.** TEM images of (A) Fraction 1, (B) Fraction 3, (C) Fraction 6, and (D) Fraction 10 corresponding to the average particle sizes of 1.6, 1.8, 2.5, and 3.1 nm, respectively. The insets display their enlarged TEM images and the selected area electron diffraction patterns, respectively.

as 2-amino-3,4,6-trihydroxyhexanal. Some minor *m*/*z* spacings 15, 16, 17, and 18 are also found in each group of fragment ions, corresponding to the mass loss of a methyl ($CH_3$), an amino ($NH_2$), a hydroxyl (OH) group, and a water ($H_2O$) molecule, respectively. Similarly, the expanded MS of Fraction 2 (Fig. 5B) displays the major *m*/*z* spacing in the alternating mass units of 115 and 169. The 115 mass spacing corresponds to one opening pyranose ring chitosan dehydrated with the loss of $H_2O$ and $–CH_2OH$ to produce 2-amino-3-hydroxypent-4-enal. The 169 mass spacing corresponds to one opening pyranose ring chitosan dehydrated with the loss of two $H_2O$ molecules and its $–NH_2$ group reacts with a $CH_3COOH$ molecule to release N-(6-hydroxy-1-oxohexa-3,4-dien-2-yl)acetamide. Some minor *m*/*z* spacings 12, 15, 17, and 18 are observed in each group of fragment ions, corresponding to the mass loss of a carbon (C) atom, $CH_3$, OH, and $H_2O$, respectively. The MS analyses of other fractions behave similarly either to that of Fraction 1 or 2. The loss of hydroxymethyl ($–CH_2OH$) functionality is also common to the fractions attributing to its surface-attachment to the analogous sphere of carbon core [8,23,38,39].

For comparison, the MALDI-TOF MS of chitosan and chitosan/acetic acid without the hydrothermal carbonization process are shown in Fig. S5A and B, respectively. Chitosan shows regular major peak spacing of 161 units, corresponding to the loss of one whole pyranose ring chitosan. For chitosan/acetic acid, the major peak spacings of 119 (118) corresponding to the loss of a $–CH_2CH_2OH$ unit during the pyranose ring opening of chitosan. The 163 spacing unit is attributed only to the pyranose ring opening of chitosan. These results demonstrate that the pyranose ring chitosan reacts readily with acetic acid with a concomitant degradation of the chitosan chain and the pyranose ring. By

contrast, Fractions 1–12 only show major spacings of 115, 163, 169, and 175 mass units (Fig. S5C and D), indicating that the pyranose ring chitosan has already reacted with acetic acid through the hydrothermal carbonization process. Again, some minor *m*/*z* spacings 12, 15, 16, 17, 18, and 32 corresponding to the loss of C, $CH_3$, $NH_2$, OH, $H_2O$, and $CH_3OH$, respectively are commonly found in each group of fragment ions for Fractions 1–12 (Fig. S6). In summary, our MS concur with the IR data (vide supra) that the C-NanoD species should comprise carbon cores with surface-attached $NH_2$, OH, and $CH_2OH$ functionalities.

### 3.4. Transmission electron microscopy of C-NanoD fractions

Since Fractions 1, 3, 6, and 10 possess some intense absorption signals that the concentration of C-NanoD species in these fractions are relatively higher, it is easier to capture their TEM images. Fig. 6 shows their TEM images and the insets show their enlarged TEM images, respectively. The average C-NanoD particle size which is obtained by counting randomly 100 particles from various spots of the fractions during TEM imaging increases in the order: Fraction 1 (1.6 nm) < Fraction 3 (1.8 nm) < Fraction 6 (2.5 nm) < Fraction 10 (3.1 nm). Again, the TEM results show that an as-synthesized C-NanoD product indeed comprises C-NanoD of various core sizes. The smaller C-NanoD species are eluted first and followed by the larger ones in RP-HPLC. The selected area electron diffraction patterns of these fractions (the bottom right insets in Fig. 6A–D) do not show well defined crystal planes, indicating the poor crystalline nature of C-NanoD species which comprise amorphous carbon atoms.

## 4. Conclusion

We have developed a RP-HPLC methodology to fractionate and study a complex mixture of the as-prepared amino/hydroxyl-functionalized fluorescent C-NanoD product. The separation coupled with UV–vis absorption, fluorescence, MS and TEM proves to be extremely useful in identifying the core size, spectral feature, characteristics and structural features of C-NanoD fractions present in the sample. The elution order follows approximately with their core sizes from the smallest to the largest. The structure of C-NanoD is a carbon core covered with $-NH_2$, –OH and $-CH_2OH$ functionalities. More importantly, our proposed RP-HPLC methodology provides well-defined peaks and should open new, convenient and rapid avenues to isolate different C-NanoD fractions for their characterization, catalysis, photophysical and other studies. Currently, the as-synthesized C-NanoD products are far from ideal in terms of purity, leaving plenty of room for the development of better analytical separation techniques to more precisely harvest various C-NanoD fractions for specific applications.

## Acknowledgments

Financial supports from the Hundred Talent Programme of Shanxi Province, HKBU Faculty Research Grant (FRG1/13–14/039) and National Natural Science Foundation of China (21175086) are gratefully acknowledged. We would express our sincere thanks to Ms. Winnie Y.K. Wu of the Institute of Advanced Materials for taking the TEM images and Ms Silva T. Mo of the Department of Chemistry, Hong Kong Baptist University for acquiring the MALDI-TOF MS. The TEM was supported by the Special Equipment Grant from the University Grants Committee of the Hong Kong Special Administrative Region, China (Grant SEG_HKBU06).

## Appendix A. Supporting information

Supplementary data associated with this article can be found in the online version at http://dx.doi.org/10.1016/j.talanta.2014.04.008.

## References

[1] S.-T. Yang, L. Cao, P.G. Luo, F. Lu, X. Wang, H. Wang, M.J. Meziani, Y. Liu, G. Qi, Y.-P. Sun, J. Am. Chem. Soc. 131 (2009) 11308–11309.
[2] S.N. Baker, G.A. Baker, Angew. Chem. Int. Ed. 49 (2010) 6726–6744.
[3] A.S. Zyubin, A.M. Mebel, M. Hayashi, H.C. Chang, S.H. Lin, J. Phys. Chem. C 113 (2009) 10432–10440.
[4] T.-S. Lim, C.-C. Fu, K.C. Lee, H.-Y. Lee, K. Chen, W.-F. Cheng, W.W. Pai, H.-C. Chang, W. Fann, Phys. Chem. Chem. Phys. 11 (2009) 1508–1514.
[5] S. Mitra, S. Chandra, T. Kundu, R. Banerjee, P. Pramanik, A. Goswami, RSC Adv. 2 (2012) 12129–12131.
[6] J. Shen, Y. Zhu, X. Yang, C. Li, Chem. Commun. 48 (2012) 3686–3699.
[7] L. Cao, X. Wang, M.J. Meziani, F. Lu, H. Wang, P.G. Luo, Y. Lin, B.A. Harruff, L.M. Veca, D. Murray, S.-Y. Xie, S.-P. Sun, J. Am. Chem. Soc. 129 (2007) 11318–11319.
[8] S.C. Ray, A. Saha, N.R. Jana, R. Sarkar, J. Phys. Chem. C 113 (2009) 18546–18551.
[9] B. Zhu, S. Sun, Y. Wang, S. Deng, G. Qian, M. Wang, A. Hu, J. Mater. Chem. C 1 (2013) 580–586.
[10] Y.-P. Sun, B. Zhou, Y. Lin, W. Wang, K.A.S. Fernando, P. Pathak, M.J. Meziani, B.A. Harruff, X. Wang, H. Wang, P.G. Luo, H. Yang, M.E. Kose, B. Chen, L.M. Veca, S.-Y. Xie, J. Am. Chem. Soc. 128 (2006) 7756–7757.
[11] X. Wang, L. Cao, S.-T. Yang, F. Lu, M.J. Meziani, L. Tian, K.W. Sun, M.A. Bloodgood, S.-P. Sun, Angew. Chem. Int. Ed. 49 (2010) 5310–5314.
[12] J. Xu, S. Sahu, L. Cao, C.E. Bunker, G. Peng, Y. Liu, K.A.S. Fernando, P. Wang, E.A. Guliants, M.J. Meziani, H. Qian, Y.-P. Sun, Langmuir 28 (2012) 16141–16147.
[13] J.S. Baker, L.A. Colón, J. Chromatogr. A 1216 (2009) 9048–9054.
[14] D. Pan, J. Zhang, Z. Li, C. Wu, X. Yan, M. Wu, Chem. Commun. 46 (2010) 3681–3683.
[15] A.B. Bourlinos, A. Stassinopoulos, D. Anglos, R. Zboril, V. Georgakilas, E.P. Giannelis, Chem. Mater. 20 (2008) 4539–4541.
[16] H. Liu, T. Ye, C. Mao, Angew. Chem. Int. Ed. 46 (2007) 6473–6475.
[17] L. Tian, D. Ghosh, W. Chen, S. Pradhan, W. Chang, S. Chen, Chem. Mater. 21 (2009) 2803–2809.
[18] Y.-P. Sun, X. Wang, F. Lu, L. Cao, M.J. Meziani, P.G. Luo, L. Gu., L.M. Veca, J. Phys. Chem. C 112 (2008) 18295–18298.
[19] J. Zhou, C. Booker, R. Li, X. Zhou, T.-K. Sham, X. Sun, Z. Ding, J. Am. Chem. Soc. 129 (2007) 744–745.
[20] H. Zhu, X. Wang, Y. Li, Z. Wang, F. Yang, X. Yang, Chem. Commun. (2009) 5118–5120.
[21] A. Jaiswal, S.S. Ghosh, A. Chattopadhyay, Chem. Commun. 48 (2012) 407–409.
[22] S. Chandra, S.H. Pathan, S. Mitra, B.H. Modha, A. Goswami, P. Pramanik, RSC Adv. 2 (2012) 3602–3606.
[23] Y. Yang, J. Cui, M. Zheng, C. Hu, S. Tan, Y. Xiao, Q. Yang, Y. Liu, Chem. Commun. 48 (2012) 380–382.
[24] J.C. Vinci, L.A. Colón, Anal. Chem. 84 (2012) 1178–1183.
[25] J.C. Vinci, I.M. Ferrer, S.J. Seedhouse, A.K. Bourdon, J.M. Reynard, B.A. Foster, F.V. Bright, L.A. Colón, J. Phys. Chem. Lett. 4 (2013) 239–243.
[26] J.C.G. Esteves da Silva, H.M.R. Gonçalves, Trends Anal. Chem. 30 (2011) 1327–1336.
[27] P. Yu, X. Wen, Y.-R. Toh, J. Tang, J. Phys. Chem. C 116 (2012) 25552–25557.
[28] Y. Fang, S. Guo, D. Li, C. Zhu, W. Ren, S. Dong, E. Wang, ACS Nano 6 (2012) 400–409.
[29] Z. Luo, Y. Lu, L.A. Somers, A.T.C. Johnson, J. Am. Chem. Soc. 131 (2009) 898–899.
[30] S. Zhu, Q. Meng, L. Wang, J. Zhang, Y. Song, H. Jin, K. Zhang, H. Sun, H. Wang, B. Yang, Angew. Chem. Int. Ed. 125 (2013) 4045–4049.
[31] R. Liu, D. Wu, S. Liu, K. Koynov, W. Knoll, Q. Li, Angew. Chem. Int. Ed. 48 (2009) 4598–4601.
[32] M.J. Krysmann, A. Kelarakis, P. Dallas, E.P. Giannelis, J. Am. Chem. Soc. 134 (2012) 747–750.
[33] X. Zhai, P. Zhang, C. Liu, T. Bai, W. Li, L. Dai, W. Liu, Chem. Commun. 48 (2012) 7955–7957.
[34] K. Scott, S.K. Cushing, M. Li, F. Huang, N. Wu, ACS Nano 8 (2014) 1002–1013.
[35] Y. Zhang, S. Shuang, C. Dong, C.K. Lo, M.C. Paau, M.M.F. Choi, Anal. Chem. 81 (2009) 1676–1685.
[36] S. Xie, M.C. Paau, Y. Zhang, S. Shuang, W. Chan, M.M.F. Choi, Nanoscale 4 (2012) 5325–5332.
[37] B.H. Kim, M.J. Hackett, J. Park, T. Hyeon, Chem. Mater. 26 (2014) 59–71.
[38] J. Jeong, M. Cho, Y.T. Lim, N.W. Song, B.H. Chung, Angew. Chem. Int. Ed. 48 (2009) 5296–5299.
[39] W.K. Choi, T.Y. Ong, L.S. Tan, F.C. Loh, K.L. Tan, J. Appl. Phys. 83 (1998) 4968–4973.